Programmable exploration of magnetic states in Lieb-kagome interpolated lattices

Alejandro Lopez-Bezanilla,[1,*] Pavel A. Dub,[2] and Avadh Saxena[1]
[1]*Theoretical Division, Los Alamos National Laboratory, Los Alamos, New Mexico 87545, USA*
[2]*Chemistry Division, Los Alamos National Laboratory, Los Alamos, New Mexico 87545, USA*

(Received 1 July 2025; revised 23 September 2025; accepted 5 November 2025; published 24 November 2025)

We investigate a hybrid modeling framework in which a quantum annealer is used to simulate magnetic interactions in molecular qubit lattices inspired by experimentally realizable systems. Using phthalocyanine assemblies as a structurally constrained prototype, we model a continuous deformation from a Lieb to a kagome lattice, revealing frustration-driven disorder and magnetic field-induced reordering in the spin structure. The goal is to show how a quantum annealer can operate as a physically instantiated, programmable platform to emulate experimentally relevant lattice deformations and produce observables in a manner analogous to an experimental measurement, enabling the characterization of magnetic arrangements beyond the reach of current molecular architectures. This surrogate modeling approach offers a pathway to explore and iteratively design tunable magnetic states in synthetic materials. The synthetic design, structural characterization, and quantum simulation framework established here defines a modular and scalable paradigm for probing the limits of engineered matter across chemistry, condensed matter, and quantum information science.

DOI: 10.1103/nykx-1tsz

I. INTRODUCTION

The search for controllable, scalable quantum systems has motivated extensive work on molecular qubits, whose intrinsic spin degrees of freedom and synthetic tunability render them promising for quantum information processing and quantum simulation [1–3]. Among available molecular platforms, phthalocyanines (Pc) stand out as chemically versatile, π-conjugated macrocycles that coordinate a wide range of metal ions, forming stable complexes with well-defined spin states [4]. When combined with open-shell transition metals such as Mn, Fe, or Co [5], Pc-based complexes realize localized magnetic moments with ligand- and environment-tunable anisotropy and exchange.

A particularly appealing candidate is vanadyl phthalocyanine (VOPc), which has emerged as a prototypical spin-1/2 qubit due to long coherence times, planar geometry, and compatibility with ultrathin substrates [6,7]. On surfaces, VOPc monolayers readily self-assemble into square or quasisquare arrays [8,9], preserving the spin center and enabling real-space and spectroscopic interrogation via STM and related probes [10]. These features make Pc-based assemblies an attractive starting point for engineering two-dimensional spin lattices with experimentally anchored parameters and well-controlled environments [11–15]. Although the typical packing geometry yields a full square lattice, engineered depletion via selective desorption, tip manipulation, or templated growth can, in principle, realize Lieb-like geometries [16,17]. Global interactions can be mediated by the substrate, including exchange transmitted through the substrate's electronic structure and substrate-induced effects such as spin-orbit coupling or proximity-induced superconducting pairing [18,19].

From the standpoint of frustrated magnetism, the Lieb and kagome lattices provide a minimal pair illustrating how coordination and local constraints dictate ordering. The Lieb lattice, a depleted square network with three sites per unit cell, is bipartite and unfrustrated, supporting antiferromagnetic (AFM) order with sharp Bragg peaks in the static structure factor $S(\vec{q})$. By contrast, the kagome lattice of corner-sharing triangles imposes mutually incompatible AFM bonds, producing extensive degeneracy and frustration-driven physics [20]. Despite their topological equivalence, the difference in local coordination enforces qualitatively distinct ground states and correlation patterns. A controlled interpolation between these geometries is therefore a sensitive probe of how geometry seeds frustration, suppresses order, and shapes field responsiveness. In rigid molecular assemblies, however, post-synthesis changes to connectivity are difficult to implement *in situ*, especially shearlike deformations that continuously reshape coordination. This motivates a surrogate platform capable of scanning geometry and fields reproducibly and at scale, while returning observables that are directly comparable to experiment.

We employ a programmable quantum annealer (QA) in this role. Classical solvers, such as Monte Carlo (MC) and simulated annealing (SA) [21], are well suited to many two-dimensional classical Ising problems. Making no claim of algorithmic advantage over such methods, we use the QA as a physically instantiated, tunable surrogate capable of (i) sweeping geometry and longitudinal fields on hardware, (ii) returning large ensembles of low-energy configurations per parameter point, and (iii) assembling experimental-style observables such as $S(\vec{q})$ and magnetization [22]. In contexts where one seeks to emulate a deformation that is hard to

*Contact author: alejandrolb@gmail.com

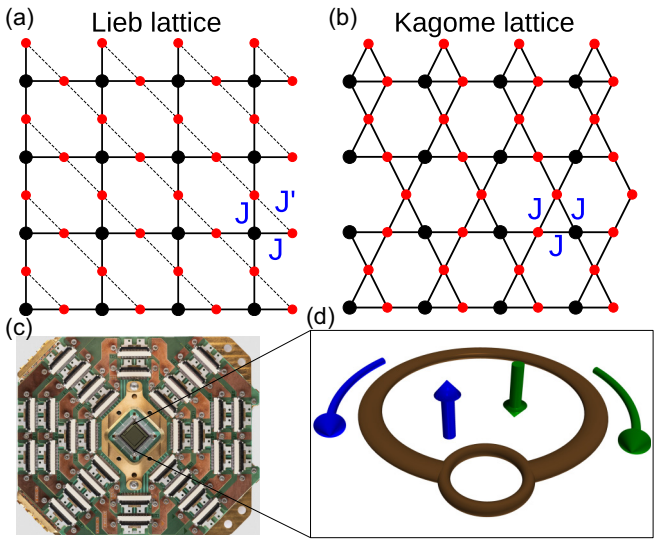

FIG. 1. Lieb lattice, (a), transforms into a kagome lattice, (b), through the application of horizontal shear strain, modeled here by a progressive increase in the coupling constant J'. The primary coupling J (between red and black nodes) initially dominates over J', until both become equal in the kagome geometry. (c) D-WAVE quantum annealing hardware used as a platform. (d) A schematic flux qubit showing opposite currents creating two different magnetic moments.

impose on an experimental lattice (e.g., a shear that converts a square-derived network toward a triangular one), the QA provides an efficient means to generate, organize, and analyze the resulting patterns of order, disorder, and field-induced reordering within a single programmable environment [23–27]. The value is thus in workflow integration: embedding an experimentally motivated model on hardware, scanning it systematically, and comparing its observables with classical calculations and future experimental data.

As a test case, we study a continuous deformation from Lieb to kagome realized by tuning a coupling asymmetry that mimics a shear of the underlying interaction graph, as shown in Fig. 1. Let J denote the AFM coupling along the "square" links and J' the AFM coupling along the diagonals [Fig. 1(a)]. Both remain antiferromagnetic throughout to isolate geometric frustration from mixed-sign effects [28]. The limit $J' \ll J$ is Lieb-like (unfrustrated), while increasing J' toward J drives the system into a kagome-like regime with maximal frustration. Further increase beyond the symmetric point distorts the triangular coordination and selects a new AFM pattern dominated by the stronger diagonal bonds. We supplement this geometric control with a tunable longitudinal field h that lifts degeneracies and selects ordered textures within frustrated manifolds. For each (J, J', h) we collect hardware samples and compute $S(\vec{q})$ and the average magnetization $\langle|m|\rangle$, thereby charting the evolution of order across the Lieb-kagome path.

Our focus in this proof of concept is the classical Ising limit (zero transverse field), so that the observed behavior reflects only the interplay of lattice geometry and the longitudinal field. This isolates the geometric mechanism underpinning frustration, degeneracy, and field selection without conflating it with quantum fluctuations. The same embedding infrastructure, however, is directly compatible with extensions that interrogate quantum regimes by schedule shaping and freeze-out analysis; such studies are outside the present scope but are natural next steps. More generally, the QA-based workflow we articulate is designed to complement classical solvers rather than to supplant them: hardware-sampled low-energy ensembles can seed or benchmark classical refinement, while classical calculations can calibrate and constrain the parameter regions explored in hardware.

II. METHODS

To simulate the magnetic behavior of geometrically evolving lattices, we encode a set of antiferromagnetically coupled spin-1/2 qubits onto the quantum processing unit (QPU) of a QA, using a time-dependent transverse-field Ising model of the form

$$\mathcal{H}(s) = \mathcal{J}(s)\left(\sum_i h_i\sigma_i^z + \sum_{i,j} J_{ij}\sigma_i^z\sigma_j^z\right) - \Gamma(s)\sum_i \sigma_i^x, \quad (1)$$

where $\mathcal{J}$ and Γ define the annealing schedule, J_{ij} encodes the pairwise interaction between qubits i and j, and h_i represents a local longitudinal field applied on the ith node. The transverse field takes the system to a quantum superposition of states to subsequently collapse it into a classical state defined by a manifold of ± 1 variables. Here σ^x and σ^z are Pauli operators. The anneal process is controlled by the relative magnitude of classical $\mathcal{J}(s)$ and quantum $\Gamma(s)$ energy scale functions. During forward annealing and according to the evolution of the unitless annealing parameter s, $\Gamma(s = 0)$ starts at its maximum while $\mathcal{J}$ vanishes. The process finishes when the transverse field is completely suppressed, $\Gamma(s = 1) = 0$, and the state stops evolving.

This formulation allows direct control over the strength and topology of spin couplings as well as the external symmetry-breaking terms. Through successive embeddings, we progressively transform a square Lieb lattice—composed of fourfold and twofold coordinated qubits—into a triangular kagome lattice characterized by fourfold coordination throughout (except for those nodes at the boundaries). This deformation is parametrized by tunable coupling sets of J and J' that govern the strength of the links exclusive to the Lieb lattice and act as a knob for inducing frustration. In contrast to real molecular systems where physical distortions result in unpredictable local fields and defect configurations, the annealer operates in a defect-free environment with precise qubit connectivity, offering a level of isolation and parameter fidelity unachievable in typical condensed matter systems. The resulting spin textures are interrogated via postannealing readouts of qubit states, allowing us to reconstruct the real-space spin configurations, compute the average magnetization, and calculate static structure factors across a range of geometries and field conditions. This methodology provides a powerful route to directly visualize how topological equivalence can mask dramatically different magnetic behavior—a distinction that is crucial for both theoretical understanding and the practical design of programmable quantum materials.

Our system consists of 913 interconnected logical spins embedded on D-Wave's Advantage system. Each logical spin is constructed from three qubits coupled ferromagnetically with a coupling strength of $J_{FM} = -2$, enabling the embedding of higher-connectivity problem graphs onto the limited native connectivity of the quantum hardware. The total number of qubits used in this study is 2739. The embedding and annealing-schedule procedures follow standard implementations that have been widely documented in the literature; detailed specifications of similar embeddings can be found, for example, in Refs. [27,29] and related works. The reference coupling between constant-length triangle sides is $J = 0.6$. In all cases we fix that J value as a reference energy scale and sweep J'. The point of maximal degeneracy is then reached when $h = J = J'$, i.e., when all couplings and the longitudinal field are equal. This convention keeps the hardware mapping transparent while preserving consistency with the usual $J'/J = 1$ condition used in the literature. J' ranges from 0.3 to 1.7. The Hamiltonian defining a classical state is

$$H(s) = \sum_{i,j} J'\sigma_i^z\sigma_j^z + \sum_{i,k} J\sigma_i^z\sigma_k^z, \tag{2}$$

where i and j are two neighboring spins (sitting at the red dots of Fig. 1) coupled by J', and i and k are two neighboring spins coupled by J. The progressive deformation of one lattice into the other can be regarded as a continuous variation of J' between a small value compared to J (Lieb lattice) up to $J' = J$ (kagome lattice) and beyond ($J' > J$), where red-dot chains in Fig. 1 become predominantly AFM.

To analyze spatial correlations and identify emergent symmetries, we compute the structure factor in momentum space as a postprocessing tool applied to the spin configurations returned by the QA. The static structure factor, $S(\vec{q})$, is defined by

$$S(\vec{q}) = \frac{1}{N_s}\sum_{i,j} e^{-\vec{q}(\vec{r}_i - \vec{r}_j)}\langle \vec{s}_i \cdot \vec{s}_j \rangle, \tag{3}$$

where N_s is the number of logical spins, $\vec{q} = (q_x, q_y)$ is a generic two-dimensional vector of the reciprocal space lattice, and $\vec{r}_i - \vec{r}_j$ is the vector between spins $\vec{s}_i$ and $\vec{s}_j$. Here $\langle\cdot\rangle$ denotes the ground state expectation value. $S(\vec{q})$ helps to determine the structure of a magnetic material, including the directions in which moments point in an ordered spin arrangement, and the interaction between spins. The images we obtain are the magnetic structure analog of the image that would be obtained by neutron diffraction techniques by reconstructions of the radiation scattered by the object [30].

When interpreting $S(\vec{q})$, it is important to use the reciprocal lattice appropriate to the underlying direct geometry. For deformations near the Lieb limit we analyze $S(\vec{q})$ in the square Brillouin zone, while near the kagome-like regime we analyze it in the hexagonal Brillouin zone associated with triangular coordination. Presenting both viewpoints highlights how the same real-space spin textures project differently in momentum space as the lattice transforms and it clarifies the appearance of diffuse boundaries and symmetry-selective peaks as frustration grows and is subsequently lifted by h.

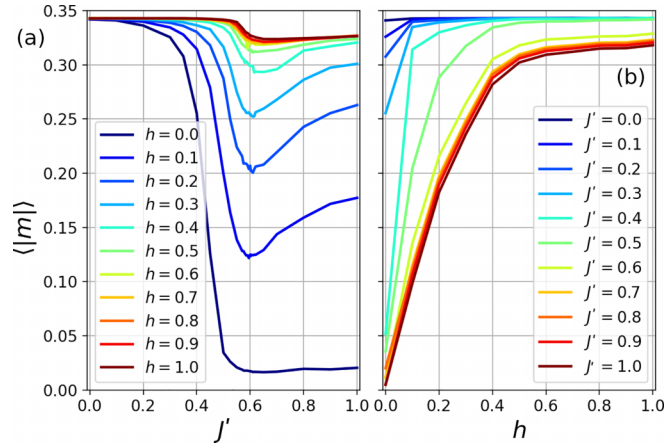

FIG. 2. (a) Evolution of the absolute value of average magnetization for different values of the local longitudinal field h with J' mimicking a finite Lieb lattice distortion. A value of $J = 0.6$ defines the coupling between magnetic moments in horizontal and vertical lattice lines (see Fig. 1). Minimum of each $\langle|m|\rangle$ is found when $J' = J$. Panel (b) shows the evolution of $\langle|m|\rangle$ as a function of the longitudinal field h for fixed values of J' coupling.

III. RESULTS

We start by outlining the workflow that underlies the present study and that can be transferred to other geometries. (1) Experimental anchor: select an experimentally motivated lattice family (e.g., Pc-based square packing) and identify feasible coupling and field scales [1,6,14]. (2) Model bounds: adopt purely AFM couplings J and J' and a longitudinal field h consistent with experimental constraints and coherence windows [2,7]. (3) QA sweep: embed the graph on the annealer, scan $(J'/J, h)$ to emulate a shear-like deformation and field tuning, and collect large ensembles of low-energy samples at each point. (4) Observables and comparison: compute $S(\vec{q})$ (in the square or hexagonal Brillouin zone, as appropriate) and $\langle|m|\rangle$, compare with classical calculations and prior phase diagrams where available, and identify geometry/field windows that are promising for future experimental control or synthesis [15–17]. In this configuration, the QA functions as a practical, complementary tool for studying frustration that arises from controlled geometric deformation and as a generator of surrogate data sets that can guide and be constrained by experiment. The present Lieb-to-kagome study illustrates this approach in its simplest form; extensions to other bipartite-nonbipartite pairs and to models with additional couplings or anisotropies follow naturally within the same framework.

Figure 2 shows how frustration, symmetry breaking, and external magnetic field shape the magnetic state of the system. The plot provides a quantitative analysis of the system's magnetic response by plotting the average magnetization $\langle|m|\rangle$ as a function of the lattice deformation parameter J' and as a function of the external longitudinal field h. Note that J' controls the interpolation between a Lieb lattice ($J' \lessapprox 0.6$), a kagome lattice ($J' = 0.6$), and beyond ($J' > 0.6$), an oblique lattice. Figure 3 illustrates the real-space consequences of varying the ratio J'/J, showing representative ground-state spin configurations along the geometric interpolation. Spins pointing in opposite directions are marked in blue and red,

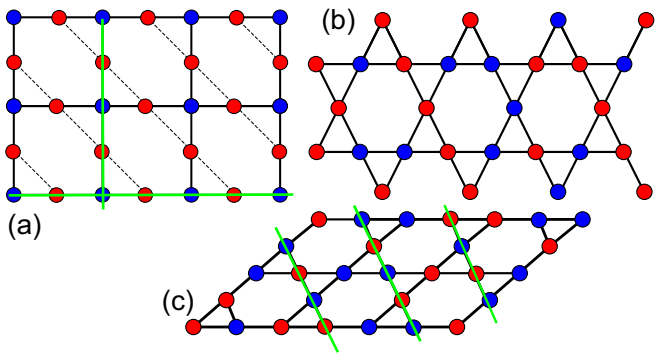

FIG. 3. Representative ground-state spin configurations obtained along the Lieb-to-kagome interpolation. Blue and red circles denote opposite spin orientations. In (a) (Lieb geometry) and (c) (distorted-kagome geometry), the green lines highlight antiferromagnetic rows that stabilize long-range order once the geometry departs from maximal frustration in (b) the kagome limit.

while green lines highlight the antiferromagnetic chains that emerge in the ordered regimes.

Each curve in Fig. 2 corresponds to a different fixed value of longitudinal field h. For $h = 0$, the system begins in an antiferromagnetically ordered state in the Lieb geometry, where magnetization is partially suppressed due to perfect spin cancellation. Figure 3(a) shows one possible ground state of perfectly alternating rows and columns of up and down spins, with frustration present only along the weak J' coupler lines. Boundary spins add a magnetization above the nominal value of 0.33. As J' increases toward 0.6, magnetic frustration is introduced, leading to a sharp drop in $\langle|m|\rangle$, consistent with the emergence of a disordered regime. This dip becomes shallower with increasing h, indicating that the external field lifts the degeneracy and restores partial magnetic ordering. At high field values ($h \geqslant 0.6$), the magnetization remains nearly constant across all values of J', suggesting that the field dominates over geometrical frustration, enforcing spin alignment regardless of underlying lattice symmetry. This panel clearly delineates a frustration-driven suppression of order at intermediate J' and low h, followed by field-induced magnetic stabilization, in excellent agreement with the structure factor evolution shown later.

Figure 2(b) provides a complementary perspective, showing how magnetization, $\langle|m|\rangle$, evolves as a function of the longitudinal field h for fixed values of J'. For small $J' = 0.35$, corresponding to a Lieb-like geometry with weak diagonal couplings ($J' < J$), the system begins in a robust AFM state. The magnetization increases slowly with h, reflecting the resistance of a nonfrustrated lattice to magnetic field-driven spin polarization. As J' increases toward $J' = 0.6$, where the diagonal and edge couplings become equal ($J = J'$) and the lattice geometry reaches the perfect kagome configuration, the system enters a maximally frustrated regime. Here, magnetization responds more rapidly to small values of h, indicating that the degeneracy of the ground-state manifold makes the system highly susceptible to symmetry-breaking fields.

Further increasing J' introduces a distortion of the kagome lattice geometry that stabilizes a different form of AFM order [Fig. 3(c)] and the magnetization curves begin to converge and saturate with increasing h. This behavior underscores the significance of the $J' = J$ point as a critical crossover in both geometry and magnetism, marking the regime of maximal frustration and strongest field sensitivity. The results reveal how the interplay between lattice connectivity and external field drives a transition from a stable antiferromagnet to a disordered, field-responsive phase. Importantly, the quantum annealer captures this tunability with precision, providing a model for how real materials could behave under controlled geometric distortions or applied fields.

Similar to conventional condensed matter techniques—such as neutron scattering or resonant x-ray scattering—a QA can produce observables but with vastly greater flexibility and efficiency. In particular, the static structure factor $S(\vec{q})$, which encodes information about spin correlations and magnetic order in momentum space, can be extracted directly from the postannealing qubit configurations for any set of model parameters. Unlike physical experiments that require sophisticated instrumentation, long measurement times, and carefully engineered samples, the QA allows us to compute $S(\vec{q})$ for an arbitrary number of configurations, geometries, and fields with minimal effort. This opens the door to a systematic, high-resolution exploration of the magnetic phase diagram across a continuous parameter space. In what follows, we present structure factor maps for a range of J' and longitudinal field h, revealing the progression from long-range AFM order in the Lieb lattice to frustrated, disordered regimes in the kagome limit.

Figure 4 presents a systematic exploration of the magnetic structure factor $S(\vec{q})$, where the $\vec{q}$ dependence of the intensity provides information on the ground-state spin correlations across a landscape defined by two key parameters: the relative diagonal coupling J' and the external longitudinal field h. The figure consists of eight columns representing different coupling ratios, with each row corresponding to an increasing value of the applied longitudinal field. From left to right, the first four columns are plotted using the reciprocal lattice of the square Lieb geometry, reflecting the square lattice symmetry in the weak-diagonal-coupling regime. In contrast, the rightmost four columns are computed using the reciprocal lattice vectors of the hexagonal (kagome) lattice, appropriate for the strong-frustration regime where the underlying direct lattice approximates triangular coordination. This shift in Brillouin zone representation enables accurate comparison of momentum-resolved spin correlations within the respective geometric frameworks, enabling us to trace a multiphase evolution of the spin system as it transitions through distinct magnetic regimes.

At $h = 0$ and a small $J' = 0.35$, the system exhibits a clean, long-range AFM order. Figure 3(a) shows a schematic of a possible realization. This is reflected in the static structure factor which displays sharp, well-defined Bragg peaks centered at high-symmetry points such as (π, π), indicating strong spin-spin correlations and a unique ground state (up to a global flip of all spins) stabilized by the bipartite lattice geometry. In this regime, the diagonal coupling J' is significantly weaker than the principal coupling J. As a result, the magnetic interactions are effectively governed by the square lattice connectivity and

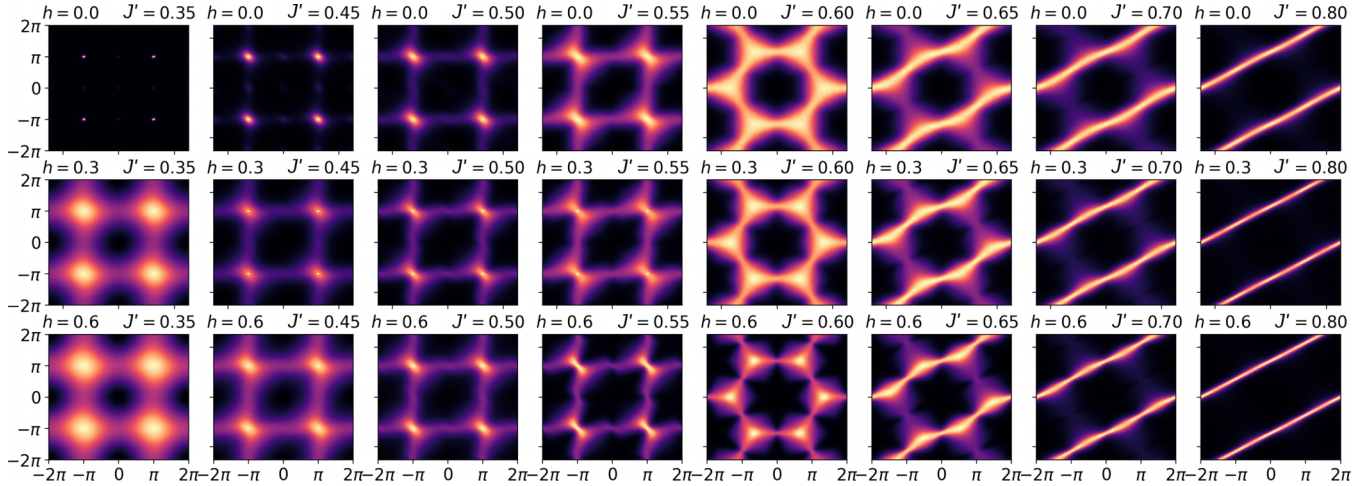

FIG. 4. Static structure factor $S(\vec{q})$ plotted for a range of coupling ratios J' and longitudinal fields h, illustrating the magnetic evolution of a spin system embedded in a programmable lattice. The first four columns are plotted using the Brillouin zone of the square Lieb lattice, while the last four use the reciprocal lattice of the hexagonal (kagome) geometry. At low J' and zero field, the system exhibits long-range AFM order with Bragg peaks at (π, π), characteristic of the crystalline Lieb lattice. Increasing J' to 0.6 suppresses this order, leading to a disordered, highly frustrated regime with diffuse correlations—indicative of a spin liquid–like state. Upon increasing h while keeping J' fixed, magnetic order is restored via magnetic field-induced crystallization, selectively favoring a subset of configurations from the degenerate manifold. Further increasing J' at constant field drives the system into a new ordered state, now governed by dominant diagonal couplings.

the weak diagonal terms do not introduce significant frustration or alter the ground-state ordering.

As the coupling J' increases to 0.6 while keeping $h = 0$, the system crosses with no phase transition into a regime of maximal magnetic disorder. The formerly crystalline structure dissolves into a diffuse $S(\vec{q})$ profile, indicative of a massively degenerate ground-state manifold. This regime corresponds to the kagome lattice, with local frustration destroying global ordering. Figure 3(b) displays the bonds forming equilateral triangles in a kagome geometry, where geometric frustration precludes long-range Néel order and the spin configuration becomes highly degenerate. It is here that the system approximates a disordered "magnetic plasma", consistent with theoretical descriptions of frustrated Ising systems [25,29].

Holding $J' = 0.6$ fixed and gradually increasing the longitudinal field h from 0 to 0.3 and 0.6 induces a re-emergence of magnetic order. The application of h breaks time-reversal symmetry and selects among previously degenerate configurations, energetically favoring specific spin arrangements. This symmetry-breaking field effectively crystallizes the disordered state into a magnetically ordered phase, as evidenced by the reappearance of well-defined intensity peaks in $S(\vec{q})$. This crystallization is analogous to magnetic field-induced ordering observed in artificial spin ice and transverse-field Ising models [25,27,31]. With the magnetic field fixed at $h = 0.6$, further increasing J' leads to another transformation in the spin texture.

As J' increases beyond 0.6, the effective geometry departs from the symmetric kagome limit, where the equilateral triangle evolves into an asymmetric scalene ($J' > 0.6$), in which the balance between edge and diagonal interactions is broken. This distortion lifts residual degeneracies and favors new spin alignment patterns, effectively selecting a different AFM ground state stabilized by a dominant diagonal J' coupling that controls the strength and spatial extent of spin correlations. Figure 3(c) shows the system in a distorted-kagome geometry where the strongest diagonal couplings dominate, stabilizing a collinear AFM state with stripe-like order along the favored bonds.

This is a different but still structured ordering pattern distinct from the initial Lieb limit but no longer disordered. The result is a third magnetic crystal, shaped not by field selection but by lattice-driven interaction hierarchy, as observed in the last column of Fig. 4.

This evolution reveals the power of combining geometrical and field-based controls within a quantum annealing framework. It shows how a programmable quantum system can emulate not only ground states but also transitions between fundamentally different magnetic regimes—ranging from highly ordered to maximally frustrated, and back into recrystallized or field-pinned configurations. In doing so, it provides insight into the subtle interplay between lattice symmetry, frustration, and external perturbations—offering an experimental venue to probe possible phase transitions that are difficult to realize or resolve in actual materials. Notably, the fact that both field and geometry can independently drive or stabilize order opens a design space where synthetic spin models can be crafted to explore nontrivial emergent behavior and test theoretical models of frustration-induced magnetism under controlled conditions.

IV. CONCLUSIONS

We have proposed and implemented a hybrid approach in which a QA is used to model interaction patterns and magnetic responses that could be observed in molecular qubit systems that are experimentally realizable but structurally rigid. Using a realistic Lieb-like geometry as the point of departure, we emulate a continuous deformation toward frustrated kagome configurations and investigate the evolution

of spin correlations and field response across this geometric manifold. The static structure factor and magnetization profiles reveal smooth configuration transitions driven by frustration and symmetry breaking, including disorder-induced suppression of magnetic order and field-stabilized crystallization of degenerate spin configurations. This interpolation does not represent a thermodynamic phase transition, but rather a smooth crossover between two topologically equivalent lattices. The suppression and subsequent reemergence of order therefore appear gradually in the observables we compute, reflecting changes in coordination geometry rather than singularities in the free energy.

Our results show strong qualitative agreement with previous classical studies of the distorted kagome Ising model, most notably the tensor renormalization-group analysis presented by Li *et al*. [28]. In particular, the phase structure and field-induced transitions we observe align closely with the regimes mapped in their Fig. 5(c), lending credibility to our quantum annealer-based implementation. However, a critical distinction lies in the interaction signs: in Li *et al*., the two competing couplings J and J' are of opposite sign, with J' explicitly ferromagnetic. This leads to ferrimagnetic or partially ordered ground states driven by sign frustration. In contrast, our model conserves antiferromagnetism throughout the lattice, with both J and J' remaining strictly antiferromagnetic. This ensures that the observed frustration arises purely from geometric distortion rather than mixed-sign competition, allowing us to isolate the effect of lattice connectivity on magnetic disorder.

In our framework, rather than positioning the QA as a faster or more accurate solver for the studied model, it is considered as a physically instantiated, tunable surrogate platform that can generate experimental-style data for parameter regimes difficult to probe in the laboratory. The Lieb-to-kagome deformation analyzed here serves as a proof of concept; future work could extend this approach by combining QA sampling with classical refinement (hybrid QA-MC or QA-simulated annealing) to explore other Hamiltonians or to incorporate transverse-field effects. In this way, QA-based modeling complements classical approaches by adding a hardware-based experimental dimension to the study of frustrated spin systems.

Looking ahead, this hybrid methodology offers a scalable and modular path toward programmable quantum matter. As quantum annealing hardware evolves, offering higher connectivity, lower noise, and more expressive Hamiltonians, its modeling capacity will continue to expand. Simultaneously, advances in synthetic chemistry and atomic-scale fabrication may unlock new ways to introduce tunability into molecular lattices themselves. We envision that this approach could evolve into a feedback loop with experiments, where measured parameters from molecular assemblies would inform QA embeddings and QA results could in turn suggest promising experimental modifications. In this vision, QAs do not merely model what already exists; they help chart the landscape of what could be made next, bringing us closer to a design framework in which molecular synthesis and quantum simulation coevolve in pursuit of functional quantum materials.

ACKNOWLEDGMENTS

A.L.B. is grateful to S. Crooker for engaging discussions and thoughtful input. Research presented in this article was supported by the Laboratory Directed Research and Development (LDRD) program of Los Alamos National Laboratory (LANL) under Projects No. 20200056DR and No. 20240343ER. Los Alamos National Laboratory is managed by Triad National Security, LLC, for the National Nuclear Security Administration of the U.S. Department of Energy under Contract No. 89233218CNA000001.

DATA AVAILABILITY

The data that support the findings of this article are available from the authors upon reasonable request.

[1] M. D. Jenkins *et al.*, A scalable architecture for quantum computation with molecular nanomagnets, Dalton Trans. **45**, 16682 (2016).

[2] A. Kamlapure, L. Cornils, J. Wiebe, and R. Wiesendanger, Engineering the spin couplings in atomically crafted spin chains on an elemental superconductor, Nat. Commun. **9**, 3253 (2018).

[3] Y. Peng, F. Pientka, L. I. Glazman, and F. von Oppen, Strong localization of majorana end states in chains of magnetic adatoms, Phys. Rev. Lett. **114**, 106801 (2015).

[4] C. Urdaniz, S. Taherpour, J. Yu, J. Reina-Galvez, and C. Wolf, Transition-metal phthalocyanines as versatile building blocks for molecular qubits on surfaces, J. Phys. Chem. A **129**, 2173 (2025).

[5] T. Suzuki, M. Kurahashi, X. Ju, and Y. Yamauchi, Spin polarization of metal (Mn, Fe, Cu, and Mg) and metal-free phthalocyanines on an Fe(100) substrate, J. Phys. Chem. B **106**, 11553 (2002).

[6] L. Malavolti *et al.*, Tunable spin–superconductor coupling of spin 1/2 vanadyl phthalocyanine molecules, Nano Lett. **18**, 7955 (2018).

[7] M. Kavand *et al.*, A general and modular approach to solid-state integration of zero-dimensional quantum systems, Nano Lett. **25**, 13787 (2025).

[8] Y. Jin *et al.*, Orientation control of vanadylphthalocyanine molecules deposited on Pt (111) and Au (111) surfaces, Jpn. J. Appl. Phys. **43**, 6259 (2004).

[9] P. J. Blowey *et al.*, The structure of vopc on Cu(111): Does v=o point up, or down, or both? J. Phys. Chem. C **123**, 8101 (2019).

[10] Y. Deng *et al.*, Tuning configurations and orbitals of vanadyl phthalocyanine on transition metals via surface alloy effect, J. Chem. Phys. **162**, 134702 (2025).

[11] S. Javaid *et al.*, Impact on interface spin polarization of molecular bonding to metallic surfaces, Phys. Rev. Lett. **105**, 077201 (2010).

[12] L. C. Ribeiro, V. Lopes, G. Chiappe, E. Louis, and E. V. Anda, Kondo effect in distorted titanium phthalocyanine molecules adsorbed on a Cu(110) metallic surface, J. Phys. Chem. C **128**, 8767 (2024).

[13] A. Gaita-Ariño, F. Luis, S. Hill, and E. Coronado, Molecular spins for quantum computation, Nat. Chem. **11**, 301 (2019).

[14] E. Coronado, Molecular magnetism: From chemical design to spin control in molecules, materials and devices, Nat. Rev. Mater. **5**, 87 (2020).

[15] C. Bonizzoni *et al.*, Coherent coupling between vanadyl phthalocyanine spin ensemble and microwave photons: Towards integration of molecular spin qubits into quantum circuits, Sci. Rep. **7**, 13096 (2017).

[16] B. Cui *et al.*, Realization of lieb lattice in covalent-organic frameworks with tunable topology and magnetism, Nat. Commun. **11**, 66 (2020).

[17] R. Drost, T. Ojanen, A. Harju, and P. Liljeroth, Topological states in engineered atomic lattices, Nat. Phys. **13**, 668 (2017).

[18] G. van Straaten *et al.*, Role of the central metal atom in substrate-mediated molecular interactions in phthalocyanine-based heteromolecular monolayers, J. Phys. Chem. C **122**, 8491 (2018).

[19] G. Avvisati *et al.*, Metal phthalocyanines interaction with co mediated by a moiré graphene superlattice, J. Chem. Phys. **150**, 054704 (2019).

[20] R. Moessner, S. L. Sondhi, and P. Chandra, Two-dimensional periodic frustrated ising models in a transverse field, Phys. Rev. Lett. **84**, 4457 (2000).

[21] G. E. Santoro, R. Martoňák, E. Tosatti, and R. Car, Theory of quantum annealing of an ising spin glass, Science **295**, 2427 (2002).

[22] P. Kairys *et al.*, Simulating the shastry-sutherland ising model using quantum annealing, PRX Quantum **1**, 020320 (2020).

[23] A. D. King, C. Nisoli, E. D. Dahl, G. Poulin-Lamarre, and A. Lopez-Bezanilla, Qubit spin ice, Science **373**, 576 (2021).

[24] A. D. King *et al.*, Quantum annealing simulation of out-of-equilibrium magnetization in a spin-chain compound, PRX Quantum **2**, 030317 (2021).

[25] A. Lopez-Bezanilla *et al.*, Kagome qubit ice, Nat. Commun. **14**, 1105 (2023).

[26] A. Ali *et al.*, Quantum quench dynamics of geometrically frustrated ising models, Nat. Commun. **15**, 10756 (2024).

[27] A. Lopez-Bezanilla, A. D. King, C. Nisoli, and A. Saxena, Quantum fluctuations drive nonmonotonic correlations in a qubit lattice, Nat. Commun. **15**, 589 (2024).

[28] W. Li *et al.*, Phase transitions and thermodynamics of the two-dimensional ising model on a distorted kagome lattice, Phys. Rev. B **82**, 134434 (2010).

[29] P. Narasimhan, S. Humeniuk, A. Roy, and V. Drouin-Touchette, Simulating the transverse-field ising model on the kagome lattice using a programmable quantum annealer, Phys. Rev. B **110**, 054432 (2024).

[30] S. Lovesey, *Theory of Neutron Scattering from Condensed Matter. Vol. 1. Nuclear Scattering* (Oxford, Oxford, UK, 1984).

[31] C. Nisoli, R. Moessner, and P. Schiffer, Colloquium: Artificial spin ice: Designing and imaging magnetic frustration, Rev. Mod. Phys. **85**, 1473 (2013).